IOPscience iopscience.iop.org

Home Search Collections Journals About Contact us My IOPscience

90 °C continuous-wave operation of GaInAsP/InP membrane distributed-reflector laser on Si substrate

This content has been downloaded from IOPscience. Please scroll down to see the full text.

2017 Appl. Phys. Express 10 032702

(http://iopscience.iop.org/1882-0786/10/3/032702)

View the table of contents for this issue, or go to the journal homepage for more

Download details:

IP Address: 131.112.10.178
This content was downloaded on 19/07/2017 at 18:15

Please note that terms and conditions apply.

You may also be interested in:

High-differential quantum efficiency operation of GaInAsP/InP membrane distributed-reflector laser on Si
Takahiro Tomiyasu, Takuo Hiratani, Daisuke Inoue et al.

Room-temperature continuous-wave operation of membrane distributed-reflector laser
Takuo Hiratani, Daisuke Inoue, Takahiro Tomiyasu et al.

Thermal properties of lateral-current-injection semiconductor membrane Fabry–Perot laser under continuous-wave operation
Takuo Hiratani, Kyohei Doi, Jieun Lee et al.

Low-threshold-current operation of membrane distributed-feedback laser with surface grating bonded on Si substrate
Yuki Atsuji, Kyohei Doi, Takuo Hiratani et al.

Room-temperature continuous-wave operation of GaInAsP/InP lateral-current-injection membrane laser bonded on Si substrate
Daisuke Inoue, Jieun Lee, Kyohei Doi et al.

Waveguide loss reduction of lateral-current-injection type GaInAsP/InP membrane Fabry–Pérot laser
Takahiro Tomiyasu, Takuo Hiratani, Daisuke Inoue et al.

Preliminary reliability test of lateral-current-injection GaInAsP/InP membrane distributed feedback laser on Si substrate fabricated by adhesive wafer bonding
Kai Fukuda, Daisuke Inoue, Takuo Hiratani et al.

Reliable Operation of GaInAsP/InP Distributed Feedback Laser with Wirelike Active Regions
Kazuya Ohira, Nobuhiro Nunoya, Hideki Yagi et al.

OPEN ACCESS

Applied Physics Express **10**, 032702 (2017)
https://doi.org/10.7567/APEX.10.032702

90 °C continuous-wave operation of GaInAsP/InP membrane distributed-reflector laser on Si substrate

Takuo Hiratani[1], Daisuke Inoue[1], Takahiro Tomiyasu[1], Kai Fukuda[1], Tomohiro Amemiya[2], Nobuhiko Nishiyama[1,2], and Shigehisa Arai[1,2*]

[1]Department of Electrical and Electronic Engineering, Tokyo Institute of Technology, Meguro, Tokyo 152-8552, Japan
[2]Institute of Innovative Research, Tokyo Institute of Technology, Meguro, Tokyo 152-8552, Japan

*E-mail: arai@pe.titech.ac.jp

Received January 17, 2017; accepted February 6, 2017; published online February 21, 2017

The temperature dependence of a GaInAsP/InP membrane distributed-reflector laser bonded on a Si substrate — which showed a low threshold current (0.29 mA) and a relatively high differential quantum efficiency (23% from the front side) at 20 °C — was measured. A characteristic temperature of the threshold current, T_0, of 84 K and a sub-mA threshold current operation up to 90 °C were obtained under a continuous-wave (CW) condition. Furthermore, single-mode operation up to 80 °C was also obtained. © 2017 The Japan Society of Applied Physics

Following advancements in transistor scaling, large-scale integrated circuits (LSIs) were developed.[1)] However, it is difficult to improve the overall performance by scaling because of problems at global interconnections on LSIs, such as signal delays and Joule heating.[2,3)] To overcome these problems, various approaches, such as those involving inductive coupling, differential transmission lines, optical links with photonic crystal lasers, and photodetectors,[4–6)] were proposed. Optical interconnection is an attractive approach to resolving the above issues owing to its high-density integration and low-power-consumption operation.[7)]

To realize the optical interconnection on LSIs, a low-power-consumption optical link, including light sources, waveguides, and photodetectors, is required. On-chip light sources with low-power-consumption operation have been reported, including vertical-cavity surface-emitting lasers (VCSELs),[8,9)] microdisk lasers,[10,11)] and photonic crystal lasers.[12,13)] These microcavity lasers can realize low-threshold-current operation owing to the high optical confinement into ultrasmall active regions. However, light output power is sacrificed because of the high optical confinement. To realize on-chip light sources, the problem of addressing the low light output power should be solved.

We previously proposed membrane photonic integrated circuits (MPICs) and demonstrated membrane lasers.[14,15)] The membrane structure consists of a thin semiconductor and low-refractive-index top and bottom claddings, such as air, SiO_2, and polymer-like benzocyclobutene (BCB). This structure can realize a large refractive-index difference, which engenders the high optical confinement in the active layer and enhances the modal gain. Therefore, membrane lasers are expected to be good candidates for on-chip light sources with low-power-consumption operation. Furthermore, a sufficient light output power of more than 0.16 mW for 10 Gbps data transmission with a bit error rate (BER) of 10^{-9} can be obtained by introducing a distributed-reflector (DR) structure; the light output power at one side was increased by introducing a rear distributed Bragg reflector (DBR).

The low-threshold-current operation,[16)] asymmetric light output characteristics of the DR structure,[17)] and high-speed modulation operation[18)] of membrane-distributed feedback (DFB) and DR lasers were demonstrated in previous works. However, the thermal properties of the current-injection-type membrane laser with a short cavity structure have not been sufficiently investigated in detail. Moreover, high-temperature operation is required for on-chip light sources owing to LSI heating. In a theoretical analysis, the self-heating effect and temperature dependence of membrane DFB lasers were examined.[19,20)] In experimental works, an 85 °C continuous-wave (CW) operation of an optically pumped device[21)] and a 50 °C CW operation of a current-injection-type device[16)] were demonstrated. Although the GaInAsP/InP membrane DFB laser for data center communication application demonstrated a 100 °C CW operation,[22)] the threshold current was as high as that of an on-chip light source.

In this study, the thermal properties of membrane DR lasers were investigated. Evaluations of thermal resistance and temperature dependence were conducted. A 90 °C CW operation with a sub-mA threshold current was obtained, even though the device had a high thermal resistance of 5250 K/W.

We prepared a membrane DR laser with a 20-µm-long front waveguide, a 30-µm-long active DFB section, and a 50-µm-long passive DBR section for the evaluation of thermal properties, as shown in Fig. 1(a). The stripe width of DFB and DBR sections was 1.1 µm. A 270-nm-thick core layer, including five GaInAsP quantum wells (5QWs), was used for the active DFB section. GaInAsP with a bandgap wavelength of 1.22 µm was used for the passive DBR section. The fabrication process used here was almost the same as that for a device in our previous work.[17)] The process included three-step selective-area regrowth by organometallic vapor-phase epitaxy (OMVPE) for the formation of the GaInAsP passive waveguide and pin junction with p-InP and n-InP, BCB bonding to the Si substrate, the evaporation of electrodes, and the formation of a surface grating and a current-blocking trench. In this device, a Au/Zn/Au electrode was introduced to obtain better contact for the p-electrode. A current-blocking trench was also introduced to reduce the leakage current through the passive waveguide section. The current-blocking trench was formed by photolithography and wet chemical etching at the final step of the fabrication process. The width of the etched section including the

Content from this work may be used under the terms of the Creative Commons Attribution 4.0 license. Any further distribution of this work must maintain attribution to the author(s) and the title of the work, journal citation and DOI.

© 2017 The Japan Society of Applied Physics

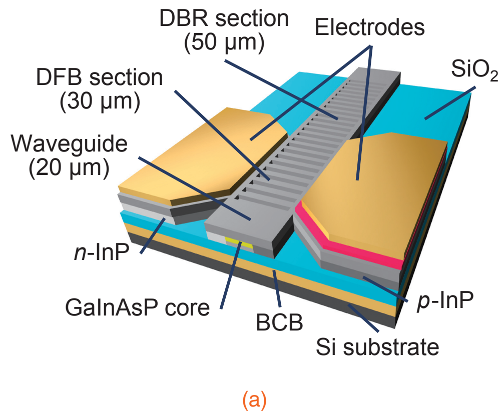

(a)

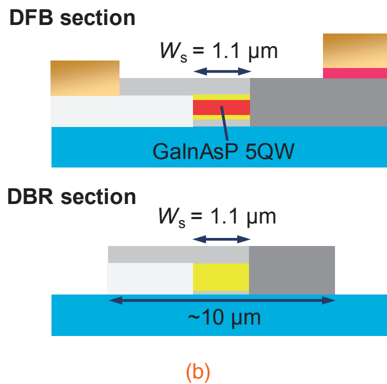

(b)

Fig. 1. (a) Schematic and (b) cross-sectional structures of membrane DR laser.

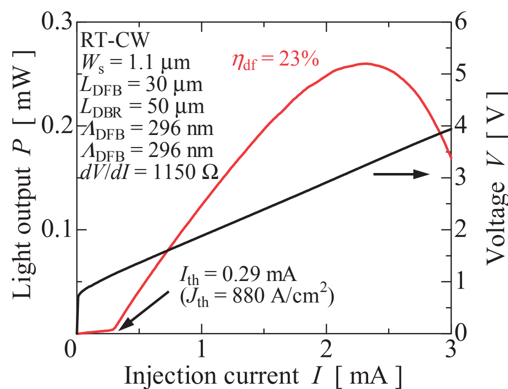

Fig. 2. Current–light output and current–voltage characteristics of fabricated membrane DR laser with a DFB section length of 30 μm.

1.1-μm-wide GaInAsP core and InP side claddings was approximately 10 μm, as shown in Fig. 1(b), and had no effect on the optical confinement in the GaInAsP core.

Figure 2 shows the current–light output (I–L) and current–voltage (I–V) characteristics of the fabricated membrane DR laser. The stripe width of the device was 1.1 μm, and the periods of both DFB and DBR sections were set to 296 nm to match the lasing and DBR Bragg wavelengths. The facets were formed by cleavage without coating. A threshold current I_{th} of 0.29 mA (corresponding threshold current density J_{th} of 880 A/cm^2), an external differential quantum efficiency from the front waveguide η_{df} of 23%, and a maximum light output power of 0.26 mW at a bias current of 2.3 mA were obtained. Compared with previous devices,

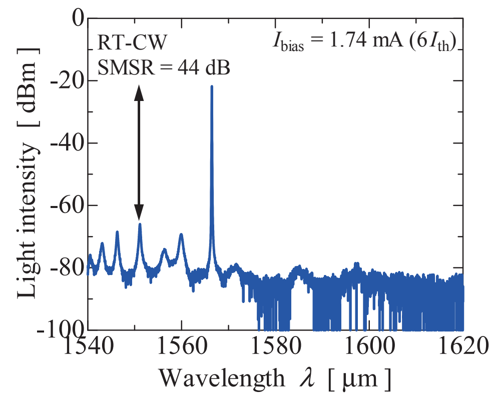

Fig. 3. Lasing spectrum under RT-CW condition.

owing to the DR structure, a low-threshold-current and high-differential-quantum-efficiency operation was realized.[16–18] Furthermore, a threshold voltage V_{th} of 1.1 V and a differential resistance of 1150 Ω were also obtained.

Figure 3 shows the lasing spectrum at a bias current of 1.74 mA ($6I_{th}$) under the room-temperature CW (RT-CW) condition. A single-mode operation with a side-mode suppression ratio (SMSR) of 44 dB at a wavelength of 1566 nm was obtained. The difference between the lasing wavelength and the gain peak wavelength was estimated to be 36 nm. The Bragg wavelength detuning effect[23] for an improved temperature dependence was expected. Although the longer wavelength mode of the stopband was not clearly observed because of the lack of optical gain, the stopband width of approximately 41 nm (corresponding index-coupling coefficient of approximately 1800 cm^{-1}) was estimated from the devices fabricated from the same wafer. A few peaks inside the stopband show Fabry–Perot resonance between the front facet and front side of the DFB section. The free spectral range (FSR) of 15 nm well agrees with that from the 20-μm-long front waveguide.

First, the thermal resistance of the membrane DR laser was investigated theoretically and experimentally. For the theoretical analysis, a typical steady-state heat transfer equation was used for calculation, as described in our previous works.[19,20] The membrane laser on a Cu heat sink (width of 11 mm and height of 2 mm) with a 2-μm-thick air gap between the laser and heat sink was assumed as the simulation model. This air gap represented the roughness between the Si substrate and the Cu heat sink. The heat sink temperature was set to 293 K as a boundary condition. The dissipation power P_{diss} was defined by the difference between the input power P_{in} and the light output power P_o, and the heat sources of P_{diss}-RI^2 for 5QWs and RI^2 for p-InP were assumed. Here, the assumption that the resistance of the p-InP side cladding region is dominant in the total device resistance[24] was used.

The thermal conductivity values in this calculation are listed in Table I; they are the same as those in our previous work.[19] Figure 4 shows the cross-sectional temperature distribution of the membrane DR laser with a 30-μm-long DFB section for the input power of 1 mW (corresponding dissipation power P_{diss} of 0.94 mW), calculated by a two-dimensional (2D) finite element method (FEM). The temperature increase of 5QWs was 7.2 K. Therefore, the esti-

© 2017 The Japan Society of Applied Physics

Table I. Thermal conductivities [W/(K·m)] used in thermal analysis.

Material	Thermal conductivity
Cu	400
Au	320
Si	158
InP	68
$Ga_{0.22}In_{0.78}As_{0.81}P_{0.19}$ (well)	5.1
$Ga_{0.26}In_{0.74}As_{0.49}P_{0.51}$ (barrier)	5.2
$Ga_{0.47}In_{0.53}As$ (Contact layer)	4.4
SiO_2	1.4
BCB	0.29

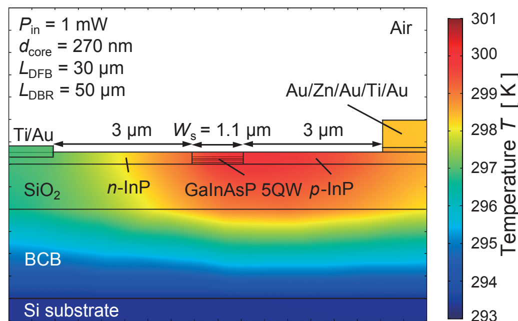

Fig. 4. Simulated cross-sectional temperature distribution of the membrane DR laser.

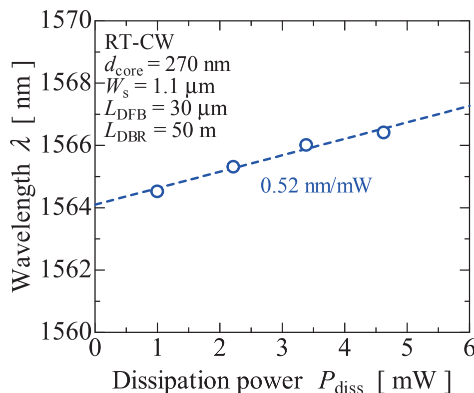

Fig. 5. Lasing wavelength as a function of dissipated power.

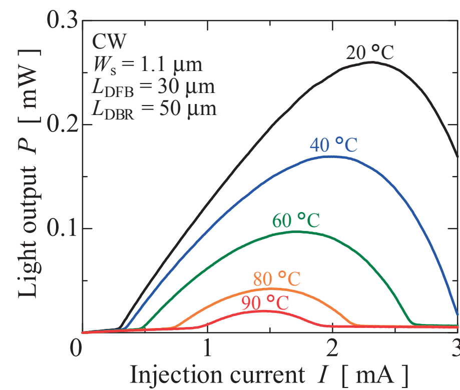

Fig. 6. Current–light output characteristics for various temperatures.

mated thermal resistance was $R_{th} = \Delta T/P_{diss} = 7600\,K/W$. This higher thermal resistance than that of conventional GaInAsP/InP lasers is a result of using cladding materials with low thermal conductivity. For on-chip application, the self-heating effect can be relatively low owing to the low operation current of the membrane laser.[19]

The thermal resistance was also estimated experimentally. We obtained $d\lambda/dP_{diss}$ of 0.52 nm/mW from the slope of the power dissipation dependence of the lasing wavelength, as shown in Fig. 5. Furthermore, $d\lambda/dT$ of 0.098 nm/K was obtained from the slope of the stage temperature dependence of the lasing wavelength under a pulse condition. As a result, the estimated experimental thermal resistance was $R_{th} = dT/dP_{diss} = (d\lambda/dP_{diss})/(d\lambda/dT) = 5250\,K/W$.

A difference exists between the obtained theoretical and experimental values. This is because the thermal diffusion to the passive waveguide section and three-dimensional (3D) FEM calculation are required to obtain accurate results. Although the device had a relatively high thermal resistance because of the 2-μm-thick BCB bonding layer with low thermal conductivity, the introduction of the thinner BCB layer could reduce the thermal resistance.[19,20]

Next, the temperature dependence of the membrane DR laser was measured. Figure 6 shows the current-light output characteristics for various temperatures. From the results, a 90 °C CW operation with a sub-mA threshold current was obtained for the first time. The improved temperature dependence compared with that of the previously reported device[16] can be attributed to the introduction of the Bragg wavelength detuning technique.[23] The temperature dependence improvement could be expected by increasing the lasing wavelength at room temperature for the gain peak wavelength.

The temperature dependences of the threshold current I_{th} and the differential quantum efficiency η_{df} were expressed by[25]

$$I_{th}(\Delta T) = I_{th0} \exp\left(\frac{\Delta T}{T_0}\right), \tag{1}$$

$$\eta_{df}(\Delta T) = \eta_{df0} \exp\left(-\frac{\Delta T}{T_1}\right), \tag{2}$$

where ΔT is the temperature increase, I_{th0} is the threshold current without self-heating, T_0 is the characteristic temperature for the threshold current, T_1 is the characteristic temperature for the differential quantum efficiency, and η_{df0} is the differential quantum efficiency without self-heating.

Figure 7 shows the threshold current and differential quantum efficiency as a function of temperature. In the temperature range from 20 to 50 °C, the characteristic temperatures T_0 of 84 K and T_1 of 114 K were obtained. Because these values are higher than typical values for GaInAsP/InP lasers, the Bragg wavelength detuning contributed to the improvement of the temperature dependence. To realize CW operation at a temperature of more than 100 °C, both the reduction in thermal resistance and the improvement of characteristic temperatures were required. Further increase in the amount of Bragg wavelength shift can improve the characteristic temperature. Finally, lasing spectra for various temperatures were measured, as shown in Fig. 8. Single-mode lasing with an SMSR of more than 40 dB was obtained up to 80 °C.

In conclusion, the thermal properties of a membrane DR laser were described in this paper. The thermal resistance

© 2017 The Japan Society of Applied Physics

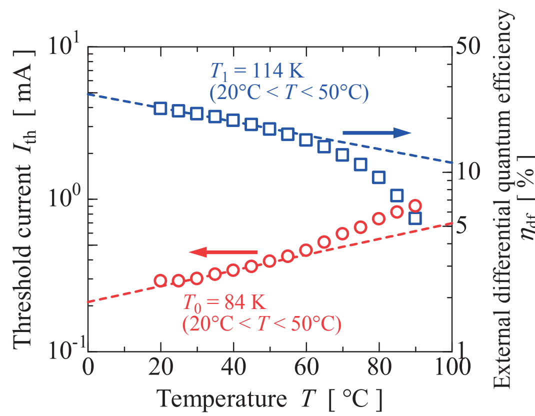

Fig. 7. Threshold current and external differential quantum efficiency as functions of temperature.

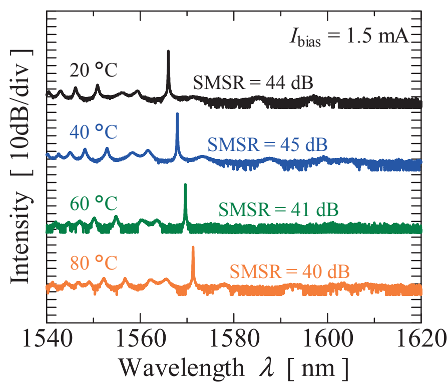

Fig. 8. Lasing spectra for various temperatures.

was theoretically and experimentally estimated to be 7600 and 5250 K/W, respectively. The device with a 30-µm-long DFB section realized a 90 °C CW operation with a sub-mA threshold current. An SMSR greater than 40 dB up to 80 °C was demonstrated. These results show the potential of the membrane DR laser for on-chip application.

Acknowledgments The authors would like to thank Professors S. Akiba, T. Mizumoto, M. Asada, Y. Miyamoto, and M. Watanabe of the Tokyo Institute of Technology for their fruitful discussions. This work was supported by JSPS KAKENHI Grant Numbers 15H05763, 25709026, 15J04654, 15J11776, and 16H06082, and JST-CREST.

1) R. H. Dennard, F. H. Gaensslen, V. L. Rideout, E. Bassous, and A. R. LeBlanc, IEEE J. Solid-State Circuits **9**, 256 (1974).
2) P. Kapur, J. P. McVittie, and K. C. Saraswat, IEEE Trans. Electron Devices **49**, 590 (2002).
3) P. Kapur, G. Chandra, J. P. McVittie, and K. C. Saraswat, IEEE Trans. Electron Devices **49**, 598 (2002).
4) N. Miura, T. Shidei, Y. Yuan, S. Kawai, K. Takatsu, Y. Kiyota, Y. Asano, and T. Kuroda, IEEE J. Solid-State Circuits **46**, 965 (2011).
5) T. Maekawa, H. Ito, and K. Masu, 34th European Solid-State Circuits Conf. (ESSCIRC 2008), 2008, p. 474.
6) T. Sato, K. Takeda, A. Shinya, M. Notomi, K. Hasebe, T. Kakitsuka, and S. Matsuo, IEEE J. Sel. Top. Quantum Electron. **21**, 728 (2015).
7) D. A. B. Miller, Proc. IEEE **88**, 728 (2000).
8) P. Moser, W. Hofmann, P. Wolf, J. A. Lott, G. Larisch, A. Payusov, N. N. Ledentsov, and D. Bimberg, Appl. Phys. Lett. **98**, 231106 (2011).
9) S. Imai, K. Takaki, S. Kamiya, H. Shimizu, J. Yoshida, Y. Kawakita, T. Takagi, K. Hiraiwa, H. Shimizu, T. Suzuki, N. Iwai, T. Ishikawa, N. Tsukiji, and A. Kasukawa, IEEE J. Sel. Top. Quantum Electron. **17**, 1614 (2011).
10) M. Fujita, R. Ushigome, and T. Baba, Electron. Lett. **36**, 790 (2000).
11) J. Van Campenhout, P. Rojo-Romeo, P. Regreny, C. Seassal, D. Van Thourhou, S. Verstuyft, L. Di Cioccio, J.-M. Fedeli, C. Lagahe, and R. Beaets, Opt. Express **15**, 6744 (2007).
12) B. Ellis, M. A. Mayer, G. Shambat, T. Sarmiento, J. Harris, E. E. Haller, and J. Vučković, Nat. Photonics **5**, 297 (2011).
13) K. Takeda, T. Sato, A. Shinya, K. Nozaki, W. Kobayashi, H. Taniyama, M. Notomi, K. Hasebe, T. Kakitsuka, and S. Matsuo, Nat. Photonics **7**, 569 (2013).
14) T. Okamoto, N. Nunoya, Y. Onodera, T. Yamazaki, S. Tamura, and S. Arai, IEEE J. Sel. Top. Quantum Electron. **9**, 1361 (2003).
15) S. Arai, N. Nishiyama, T. Maruyama, and T. Okumura, IEEE J. Sel. Top. Quantum Electron. **17**, 1381 (2011).
16) D. Inoue, J. Lee, T. Hiratani, Y. Atsuji, T. Amemiya, N. Nishiyama, and S. Arai, Opt. Express **23**, 7771 (2015).
17) T. Hiratani, D. Inoue, T. Tomiyasu, Y. Atsuji, K. Fukuda, T. Amemiya, N. Nishiyama, and S. Arai, Appl. Phys. Express **8**, 112701 (2015).
18) D. Inoue, T. Hiratani, K. Fukuda, T. Tomiyasu, T. Amemiya, N. Nishiyama, and S. Arai, Opt. Express **24**, 18571 (2016).
19) K. Doi, T. Shindo, J. Lee, T. Amemiya, N. Nishiyama, and S. Arai, IEEE J. Quantum Electron. **50**, 321 (2014).
20) T. Hiratani, K. Doi, J. Lee, D. Inoue, T. Amemiya, N. Nishiyama, and S. Arai, Jpn. J. Appl. Phys. **54**, 042701 (2015).
21) S. Sakamoto, H. Naitoh, M. Ohtake, Y. Nishimoto, T. Maruyama, N. Nishiyama, and S. Arai, Jpn. J. Appl. Phys. **46**, L1155 (2007).
22) S. Matsuo, T. Fujii, K. Hasebe, K. Takeda, T. Sato, and T. Kakitsuka, J. Lightwave Technol. **33**, 1217 (2015).
23) Y. Nishimoto, H. Yagi, K. Miura, D. Plumwongrot, K. Ohira, T. Maruyama, and S. Arai, Jpn. J. Appl. Phys. **46**, L411 (2007).
24) T. Hiratani, T. Shindo, K. Doi, Y. Atsuji, D. Inoue, T. Amemiya, N. Nishiyama, and S. Arai, IEEE J. Sel. Top. Quantum Electron. **21**, 1503410 (2015).
25) L. A. Coldren and S. W. Corzine, *Diode Lasers and Photonic Integrated Circuits* (Wiley, New York, 1995) 1st ed.

© 2017 The Japan Society of Applied Physics